Micromachined terahertz Fabry-Perot cavity highly directive antennas

Konstantinidis, Konstantinos; Feresidis, Alexandros P.; Tian, Yingtao; Shang, Xiaobang; Lancaster, Michael J.

DOI:
10.1049/iet-map.2014.0555

Document Version
Peer reviewed version

Citation for published version (Harvard):
Konstantinidis, K, Feresidis, AP, Tian, Y, Shang, X & Lancaster, MJ 2015, 'Micromachined terahertz Fabry-Perot cavity highly directive antennas', *Microwaves, Antennas & Propagation*, vol. 9, no. 13, pp. 1436-1443. https://doi.org/10.1049/iet-map.2014.0555

Micromachined Terahertz Fabry-Perot Cavity Highly Directive Antennas

K. Konstantinidis, A. P. Feresidis, Y. Tian, X. Shang, and M. J. Lancaster

School of Electronic, Electrical and Computer Engineering,
University of Birmingham,
Birmingham, B15 2TT, UK
email: kxk115@bham.ac.uk

Abstract

We present the design and implementation of a new type of micromachined terahertz planar highly directive antenna based on a periodic partially reflective surface. The periodic surface and antenna are fabricated using SU-8 photoresist micromachining technology. The proposed antenna is based on a Fabry-Perot type resonant cavity which is formed by superimposing the periodic surface over a single waveguide-fed slot in a metallic ground at a distance of about half wavelength. Simulations and measurements of the antenna performance are presented.

Index Terms—Partially Reflective Surfaces, Fabry-Perot cavity, Periodic structures, THz antennas.

1. INTRODUCTION

Periodic surfaces are passive periodic arrays of metallic elements on a substrate or apertures in a metallic screen, with the property to alter the magnitude and phase of incident electromagnetic fields according to the design of their geometrical parameters. In recent years, there has been increased interest in the design and fabrication of periodic surfaces at millimetre-wave and sub-millimetre-wave/THz frequencies for numerous applications. Periodic surfaces have been developed as Frequency Selective Surfaces (FSS) and employed as demultiplexing elements in passive Earth observation THz radiometers traditionally employing a single mechanically scanned aperture antenna [1-4]. FSSs are used in the quasi - optical receiver of these advanced instruments to spectrally separate the signals that are collected by the scanning

antenna [5]. Split slot ring based periodic surfaces have also been developed as thin linear to circular polarization converters [6]. Other applications of THz periodic surfaces include thin absorbers [7] and THz biosensors for chemical and biochemical materials [8].

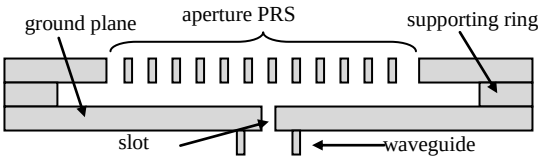

Fig. 1. Schematic diagram of the proposed antenna

THz frequencies offer new opportunities for communications, sensing and imaging applications [8, 9]. Such applications require high efficiency and high gain antennas to improve the overall system gain and enhance the signal-to-noise-ratio. At THz frequencies, reflector-based antennas [9] and horn antennas [10, 11] have been used. Despite their good radiation performance, they are bulky, which is an important drawback and furthermore they require complex, expensive and time-consuming fabrication techniques (e.g. CNC metal milling) in order to achieve the desired tolerances at these frequencies. Lenses have also been reported [12] as highly directive antennas for broadside radiation. Lens antennas are fabricated with laser silicon etching, which is not cost-efficient, and they normally have a profile of several wavelengths which is increased if a higher gain value is desired [13]. Although a profile of several wavelengths is not a problem at higher THz frequencies (over 1 THz) it can be problematic at the lower end of the THz spectrum (about 300GHz) particularly in the case of compact integrated systems. Planar antennas are therefore required for compact integrated systems at low THz frequencies [14]. In addition, planar antennas are readily compatible with micromachining techniques which lead to low-cost fabrication for mass production. Conventional microwave planar antennas employ microstrip patch arrays to achieve high gain. Nevertheless, patch arrays are not a viable solution for THz frequencies since they exhibit high losses low efficiency and narrow bandwidth. Recently, a new paradigm for the use of periodic surfaces for the realization of high gain and improved bandwidth antennas with a single feeding source has been proposed [15, 16] based on earlier work in the 1950s [17]. The antenna is based on a periodic partially reflective

surface (PRS) superimposed over a ground plane with a single radiating source (e.g. slot in the ground plane, dipole or patch). This led to increased research interest in this type of antennas [18-20] and more recently implementations in mm-wave bands [21].

In this paper, we employ low-cost SU8 photoresist micromachining technology in order to develop planar highly directive Fabry-Perot cavity antennas at approximately 300GHz. A fully metalized micromachined PRS is placed at half wavelength distance over a metallic ground and a single waveguide-fed slot (Fig. 1). The PRS is supported on a metalised SU-8 polymer ring. A resonant air cavity is thus formed with the metallic ground which leads to directive radiation patterns and high gain. The antenna, including a waveguide section feeding the resonant cavity, is implemented using micromachining fabrication techniques available at the University of Birmingham. SU-8 photoresist polymer is employed that has the advantages of high dimensional accuracy, high achievable structure aspect ratio and a capability of large scale inexpensive production. The proposed antenna supports a leaky wave mode within the cavity when excited by a single feed. A large radiating aperture is hence formed that produces directive patterns without the need for complex feeding network and associated losses. The directive beams can be broadside or tilted towards larger angles as it is demonstrated.

2. Design of THz Periodic Surface

In this section the design of the proposed periodic PRS is described. Full-wave periodic analysis is employed using CST Microwave Studio^{TM} simulation software. Periodic boundary conditions are applied to the unit cell of the structure, assuming an infinite size of the periodic surface, and reduce the calculations of the complete structure into a single unit cell. The performance of the FPC antennas that are described in later sections can be explained employing ray optics theory and is based on the reflection characteristics of the PRS [15, 17]. The analysis described in [15] shows that a high PRS reflection coefficient magnitude will result in high antenna directivity and a slow variation of the PRS reflection phase with frequency will

result in improved antenna bandwidth. Thus, the proposed PRS is designed according to the aforementioned requirements.

A square aperture PRS element has been chosen for the design. The elements are etched in a 0.432 mm thick SU-8 layer which is then silver plated as described in section 4. The dimensions of each element are 0.48x0.48 mm^2 and the periodicity is 0.6 mm (Fig. 2). The thickness of the layer was chosen in order to facilitate the micromachining fabrication process while the periodicity and the size of the aperture were selected so that the desired phase response was achieved. The simulated reflection coefficient (magnitude and phase) is obtained for normal incidence and is shown in Fig. 2. A slow variation of the phase with frequency is observed. High values for the reflection coefficient magnitude are obtained for the chosen unit cell dimensions which indicate high antenna directivity.

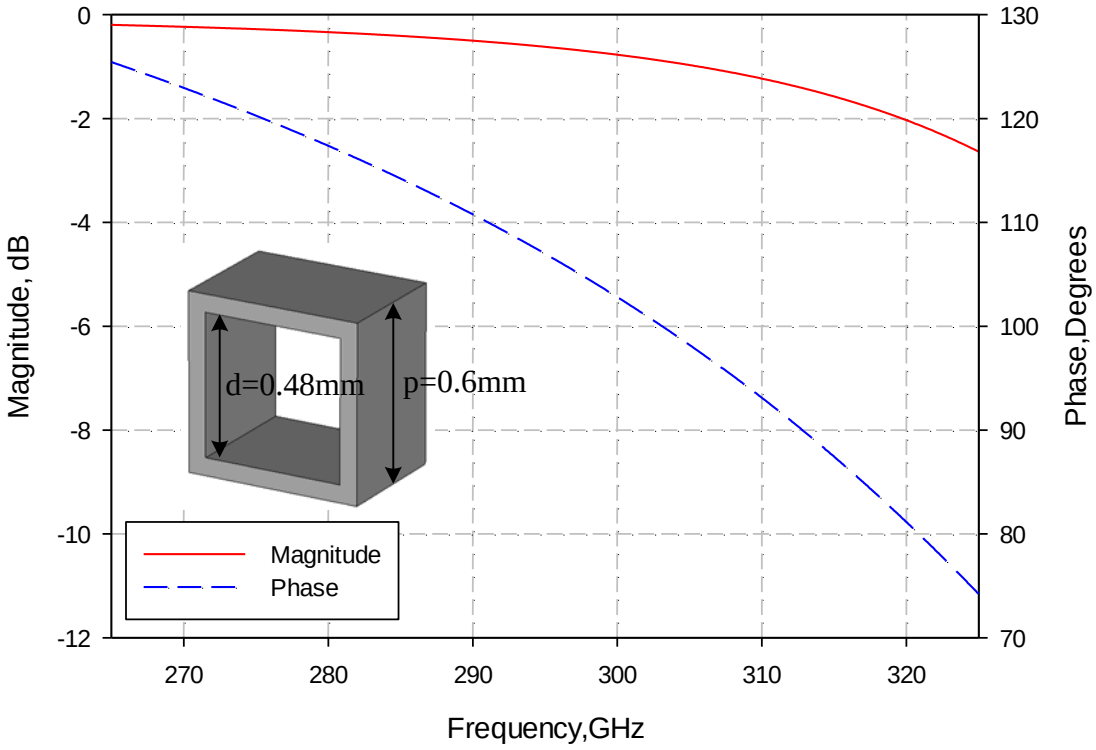

Fig. 2. Unit cell dimensions and simulated complex reflection coefficient of the proposed PRS.

3. Antenna Design

Next, a finite size antenna is designed based on the unit cell analysis of the previous section formed by a PRS array placed at half wavelength distance over a ground plane. Two back-to-back H-plane bends and a waveguide section are employed and designed in order to provide a direct and accurate connection interface with the standard waveguide [22]. One end of the bend is connected to the antenna and the other end directly to the waveguide flange. In total it is formed by three micromachined layers each of which contains holes to allow precision alignment pins and screws of the waveguide flange to pass through. The dimensions of the holes match the ones of the flange. The length of the straight section is 13.55 mm, and has been chosen in order to permit fair separation between the flange and the antenna. This ensures that the pins and screws are not blocked from the other side and do not interfere with the antenna.

The complete antenna structure comprises six metalized SU-8 layers and two brass plates placed on the top and bottom to support and hold the structure together (Fig. 3). Starting from the bottom, layers 1 to 3 form the waveguide bend described above, and layers 4 to 6 form the FPC antenna.

(a)

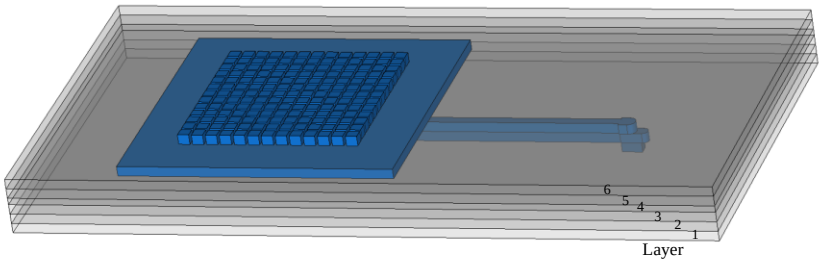

(b)

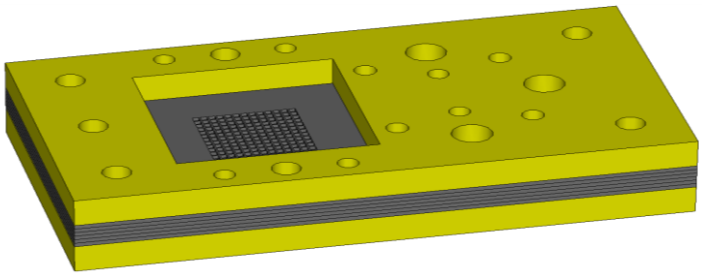

(c)

Fig.3. Diagrams of the assembled antenna. (a) The blue part represents the hollow space and the surrounding conductors were made transparent to offer a clearer view. (b) Complete structure including brass plates and holes for alignment pins and screws.

A top view of all three layers forming the bend is shown in Fig. 4(a), showing the area of interest and excluding the holes for the alignment pins and screws. In the same figure the other three layers of the structure are shown which form the FPC structure. Five of the six layers have the same thickness, equal to 0.432 mm to simplify the fabrication. However, due to restrictions explained in section 4, the thickness of the ground plane was reduced to the minimum available thickness which is 0.288 mm. The antenna's design is based on the creation of Fabry-Perot type resonant cavity as mentioned in the introduction. It is formed of a slotted ground plane (layer 4), a supporting ring that defines the air cavity thickness (layer 5) and the PRS (layer 6). The values of the parameters shown in the Fig. 4(a) are given in Table I.

In Fig. 4(b) the brass plates used to support the structure are shown. The holes have different diameters corresponding to the diameter of the screws used for clamping the structure and the pins that assure the alignment of the antenna's layers and waveguide flange. A rectangular aperture is etched for the radiation side, large enough so that it will not interfere with the performance of the antenna. From the feeding side, a circular aperture is made to fit the SU-8 device to the waveguide flange. The brass plates have a thickness of 3mm in order to make the whole structure rigid. The rest of the dimensions are also given in Table I. It is important to note that the brass plates are only used to clamp the SU-8 layers together and strengthen the structure and form no part in the alignment of the layers or waveguide flange.

The antenna has thus been formed using the optimized aperture PRS layer, placed on top of the supporting layer in front of the ground plane. An air cavity is thus created of approximately half wavelength at 300 GHz (0.432 mm). The slot in the ground plane fed from the waveguide bend is used as a single feeder of the antenna. The dimensions of the slot in the ground plane were selected such that a good matching in the frequency range of interest is achieved. For the PRS, a total of 13x13 array elements are etched into the SU-8 layer, whose total length corresponds to about 8λ at 300 GHz. Although it is a finite size structure, it is electrically large enough for the edge effects to be negligible. Moreover the distance of the supporting walls from the end of the PRS array is about 4λ. This was carefully studied by simulation to ensure that the antenna performance and the radiation patterns are not deteriorated.

The complete structure of the proposed antenna has been simulated in CST Microwave Studio and the obtained directivity and gain are presented in Fig. 5. A maximum directivity of 22.8 dBi has been achieved at 283.8 GHz with a 3 dB radiation bandwidth of approximately 4.5 GHz. The return loss is also shown in Fig. 5 with a minimum of around -20dB at 281.8 GHz, whereas at the central frequency, 284 GHz, $|S_{11}|$ is -7.5 dB. This performance could not be further optimized due to the fabrication limitations in terms of the minimum dimension of the feeding slot. Thinner feeding slots have produced S_{11} values below -15 dB. Moreover, less reflective arrays could give better performance in terms of matching, but a lower directivity would be obtained. The impedance mismatch and material losses give a deviation of 1.5 dB between directivity and gain at the central frequency.

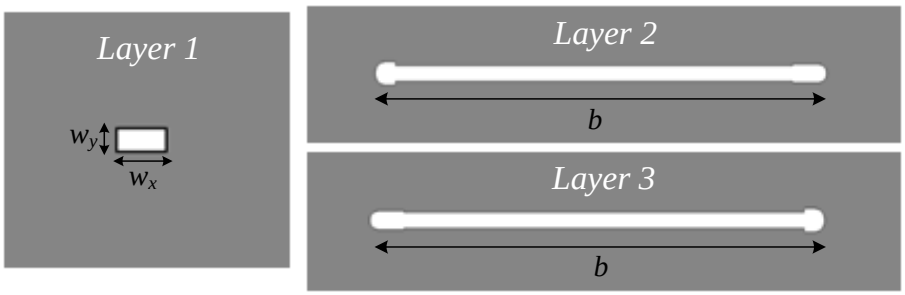

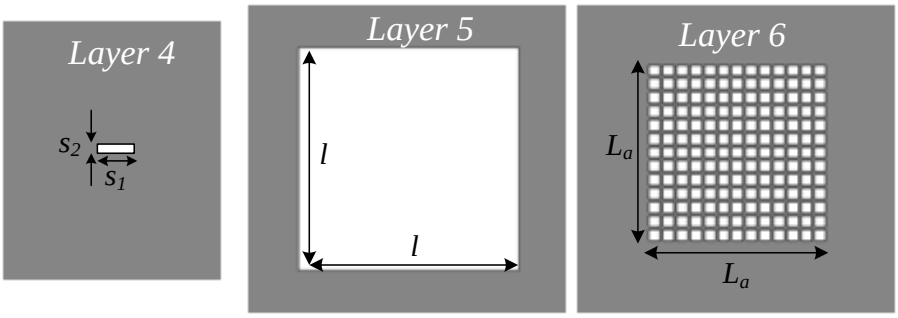

(a)

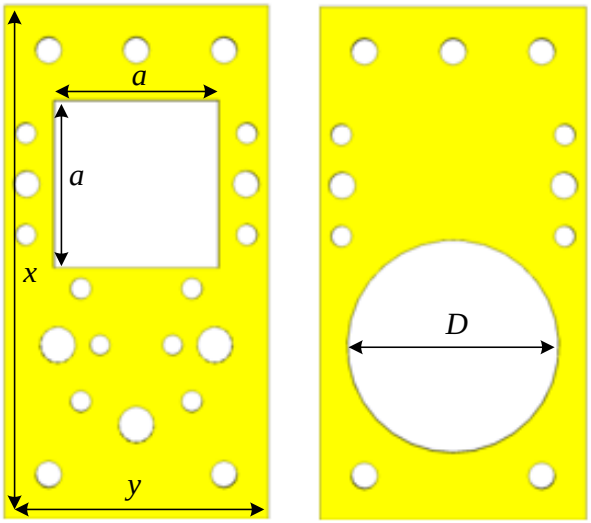

(b)

Fig. 4. (a) Illustration of the 6 layers forming the complete antenna structure (top view), white color represents the air and grey the silver, (b) Top and bottom brass plate layers.

TABLE I
ANTENNA DESIGN DIMENSIONS FROM FIG. 4

Parameter	α	x	y	D	w_x	w_y
Value (mm)	13	46	24	19.05	0.8636	0.4318
Parameter	b	s_1	s_2	l	L_a	
Value (mm)	15.4	0.5	0.09	11.8	7.68	

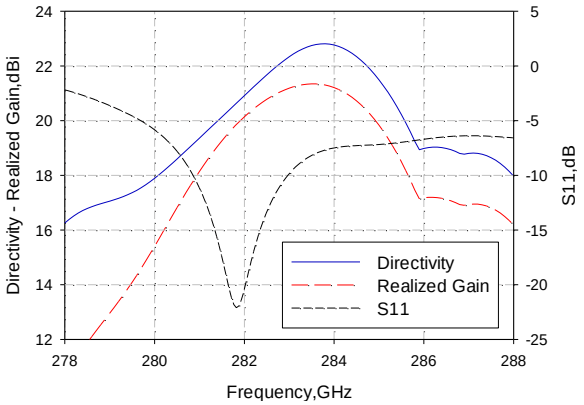

Fig. 5. Simulated directivity, realized gain and return loss of the proposed antenna.

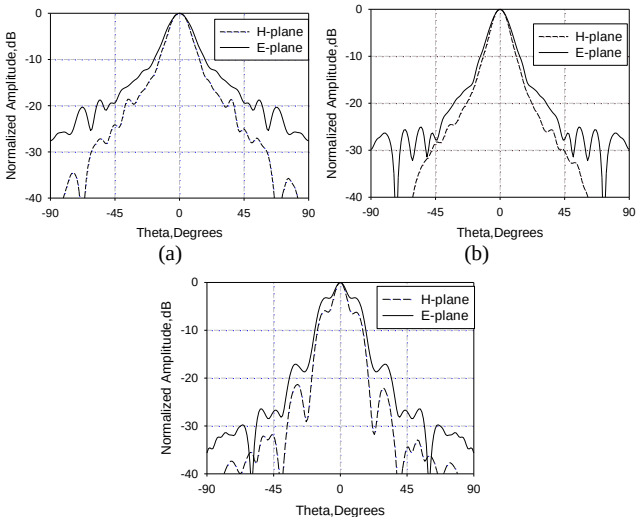

Fig. 6. Simulated H- and E-plane radiation patterns for: (a) 281GHz, (b) 283GHz and (c) 285GHz.

In Fig. 6 the H-plane and E-plane radiation patterns are shown for three frequencies over the operating band. Broadside directive beams are observed with a side lobe level below -20dB at the lower and central frequency whereas at the upper edge the beam becomes narrower with slightly higher sidelobes. This becomes more obvious at higher frequencies, were a split

beam is obtained and the maximum radiation angle increases with frequency; this again is typical for leaky-wave antennas and could be useful in certain applications requiring multi-beam and beam scanning designs. Moreover, if a straightforward change in the position of the feeding slot towards one side of the antenna is performed, a single beam radiation pattern is obtained. To validate this concept, three slot positions were considered as shown in Fig. 7(a). The simulated S_{11} for all the cases is presented in Fig. 7(b), showing a good matching between around 294GHz and 305GHz, revealing a second possible operational band of the proposed antenna. The corresponding radiation patterns for operation at 302GHz are shown in Fig. 8. It can be observed that for position 1 (Fig. 8a) there are two beams at -40^{o} and $+40^{o}$. As the slot is moved towards one edge of the antenna, one of the two beams is suppressed, as expected, resulting in a single beam at 32^{o} with good side lobe level for position 3 (Fig. 8c). Furthermore, an angle scan of 12^{o} with frequency is obtained within the frequency band where good matching is observed.

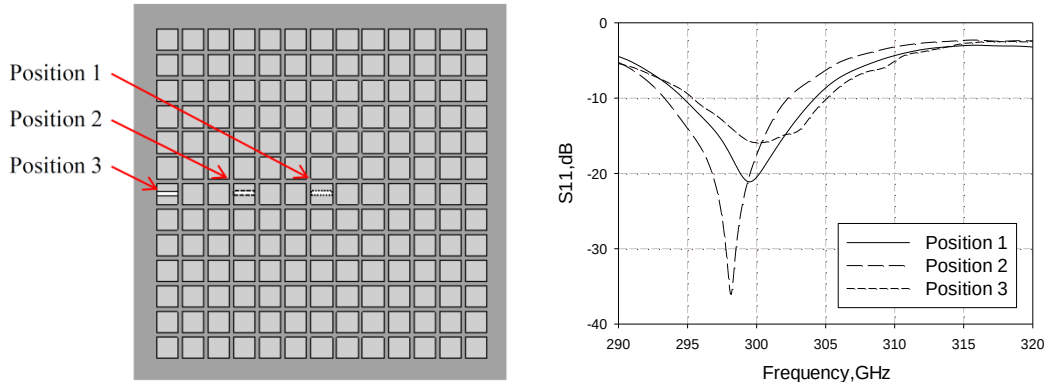

(a) (b)

Fig. 7. (a) Illustration of the three feeding slot positions (top view), (b) Simulated S_{11} for three slot positions.

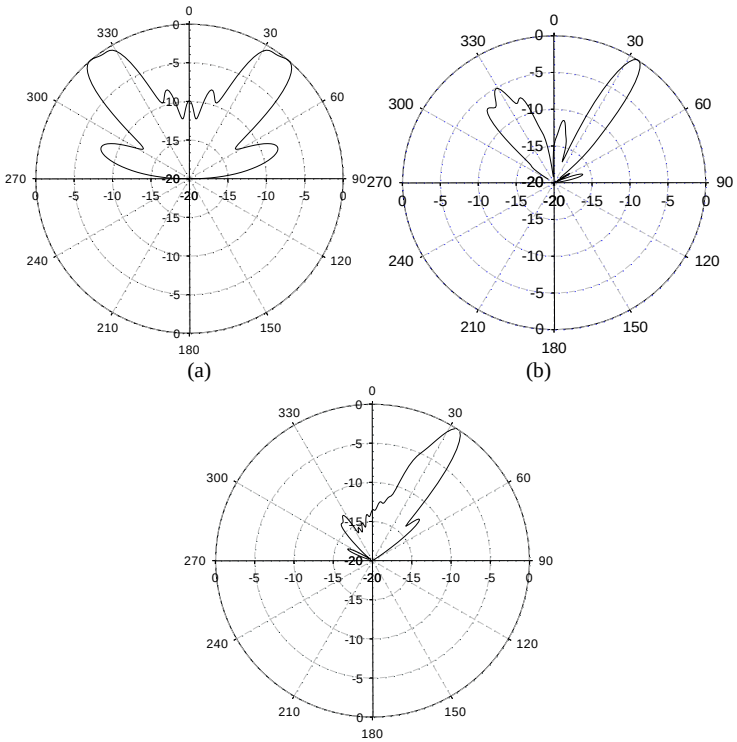

Fig. 8. Simulated H-plane radiation patterns at 302GHz for: (a) position 1, (b) position 2, and (c) position 3 (from Fig. 7).

4. Fabrication

The antenna has been designed using a square aperture PRS in a silver plated SU-8 layer. SU-8 is a UV-sensitive photoresist and able to form structures of high aspect ratio [22, 23]. The required accuracy at such high frequencies imposes the use of micromachining fabrication techniques so SU-8 is chosen as a suitable solution for this technique. A simple process is involved which can be exploited for volume production. Furthermore, the losses in silver plated SU-8 waveguiding structures are similar to those in solid metal structures and the cost of the material is low [24].

The designed antenna consists of 6 layers, as shown in Fig. 4(a) and each layer was originally designed to be 432 μm thick. However, in order to achieve better metallization inside the narrow waveguide slot, layer 3 was reduced to 288 μm as mentioned in the previous section,

to allow the silver to be coated thoroughly over all the sidewalls. All the layers were fabricated through an ultra-thick SU-8 photo-resist based micromachining process. First, SU-8 50 photo-resist was spin coated on a 100 mm silicon wafer and the edge bead was removed immediately. For the layers with different thickness, the amount of the SU-8 disposed on wafer and spin coating parameters were adjusted to achieve the desired thickness. Then, the wafer rested on a carefully leveled stage for few hours to allow the liquid resist to be self-planarized. This step is critical to harvest a smooth and uniform surface. After that, the wafer was baked at 65^{o}C and 95^{o}C subsequently and thereafter patterned with the designed mask in a Cannon PLA-501 mask aligner. For the 288 μm layer the baking time was 30 min at 65^{o}C and 2 h and 40 min at 95^{o}C. For the 432 μm layers the baking time was 30 min and 4 h and 30 min at 65^{o}C and 95^{o}C respectively. Post exposure bake was conducted at 70^{o}C, which was lower than the previous bake, to reduce the thermal stress accumulated in the thick SU-8 layer. The pieces were developed in EC solvent and released from the silicon wafer using KOH solution. Finally, the SU-8 pieces were metalized with 2 μm thick silver in a Cressington 308R vacuum evaporator.

Finally, the antenna was assembled by stacking the six silver-coated SU-8 layers and clamping between two brass plates, as illustrated in Fig. 3(b). A careful alignment of the layers had been carried out using two metallic pins with precise diameter which also acted as the dowel pins to fit into the standard waveguide flange. A photo of the assembled circuit is shown in Fig. 9.

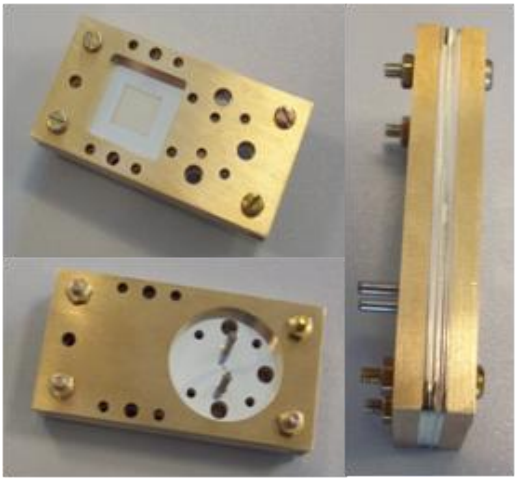

Fig. 9. Photograph of fabricated antenna comprising six layers of metallised SU-8 and brass plates.

5. Measurements

In this section, measurements of the fabricated prototype are presented. Initial measurements demonstrated that the operation of the antenna was shifted at a lower frequency than the expected one. This fact suggested that some of the dimensions of the fabricated antenna did not match the proposed design due to fabrication inaccuracies. An error of up to ±20 μm can be expected with the employed fabrication procedure, which has a significant effect in this frequency band. Another factor that could have contributed in this altered behaviour is the possible imperfect flatness of the SU-8 layers, and in particular the top radiating PRS layer. Based on the above, the antenna was simulated again in an effort to achieve better agreement with measurements and hence account for the altered fabricated dimensions.

The parameter that most significantly affects the antenna's operating frequency is the thickness of layer 5 which defines the height of the air cavity. This was increased by 30 μm. It is worth noting that the 30 μm added to the cavity height can be attributed partly to the fabrication tolerance in the thickness of layer 5 and partly to the slight curvature of layers 5 and 6. The new value of the cavity height is 462 μm.

In Fig. 10, the simulated realized gain and S_{11} is presented for the new structure. The maximum broadside gain is now shifted to 267 GHz with a value of 19.1 dBi. The matching has deteriorated, achieving only around -2 dB within the operating bandwidth. However, at higher frequencies where the beam splitting effect is observed, good matching is obtained from 294GHz to 305GHz. The maximum gain at this frequency band is 13.4dBi. However for a single beam operation with the feeding slot at one edge of the ground plane as described in section 3, the maximum gain has been calculated to be 15.9dBi which is expected since the radiated power is almost doubled.

The S-parameters were measured using an Agilent N5250A network analyzer with OML WR-3 extension head. The radiation patterns were measured in an automated anechoic chamber of 60 x 60 x 90 cm^3 dimensions available at the Rutherford Appleton Laboratory, Didcot, UK. A WR-2.8 corrugated feed horn was used as a receiver placed at a distance of 22 cm from the antenna under test. The patterns were measured only at a small number of frequencies due to allocated time limitations in order to validate the simulation predictions. At each frequency a dynamic range of more than 40 dB was achieved for the patterns measurement. Only H-plane patterns were measured. In Fig. 11(a), the comparison of the simulated and measured S_{11} is shown after having removed layer 5 and 6, in order to validate the performance of the waveguide-fed slot in the ground plane (layer 4). The antenna was carefully reassembled including the brass plates. The good agreement between simulation and measurements (less than 2% frequency shift) indicates that the dimensions of the coupling slot were only slightly altered.

The measured S_{11} response of the complete antenna structure in comparison with the simulated one for the original and the redesigned antenna is depicted in Fig. 11(b). There is a good agreement between the measured and the simulated response of the redesigned antenna.

For frequencies around 267 GHz, where the antenna is expected to operate, there is a discrepancy of about 1dB which is attributed to losses.

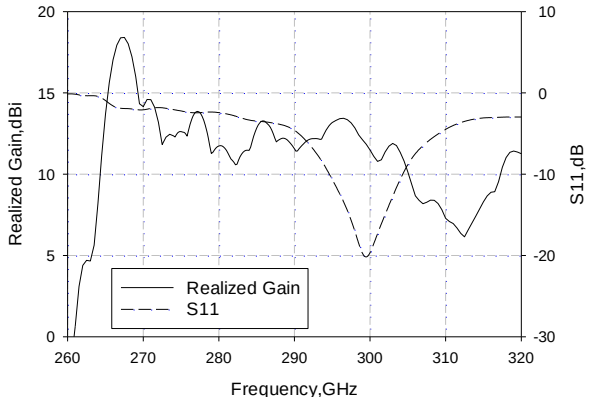

Fig. 10. Simulated realized gain and S_{11} of the redesigned antenna.

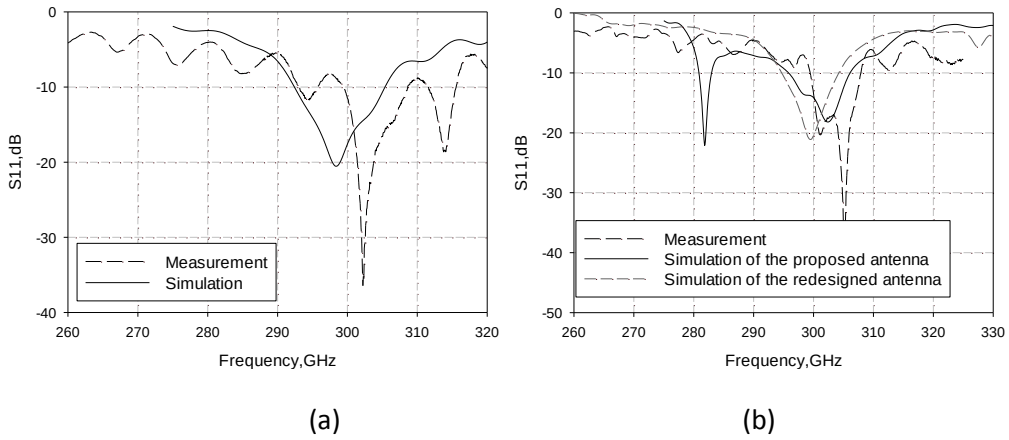

Fig. 11. (a) Measured S_{11} in comparison with simulation of ground plane with a slot, (b) Measured S_{11} in comparison with simulation of proposed and redesigned antenna.

In Fig. 12 the normalized measured H-plane patterns are shown for four different frequencies. It can be observed that there is a very good agreement with the simulations. Nevertheless, a consistent asymmetry is evident at the measured patterns, which is not present in the simulation. This is attributed to unwanted reflections at the relatively bulky positioning structure that was supporting the antenna in the measurements set-up. At the time of the radiation pattern measurements we lacked the exact information about the dimensional

discrepancies of the fabricated antenna, which as explained above led us to the redesigned antenna simulation model. However, a good directive pattern was obtained at 268GHz, i.e. very close to the central frequency of maximum broadside gain. The slightly distorted main beam is typical of this type of leaky-wave FPC antennas when operated above the central frequency as explained previously. It is interesting to note that in the frequencies where the split beam is observed, i.e. around 302GHz, the antenna is well matched (Fig. 11b). This means that it could be used for beam scanning applications applying the change in the position of the feeding slot as proposed in Section 3.

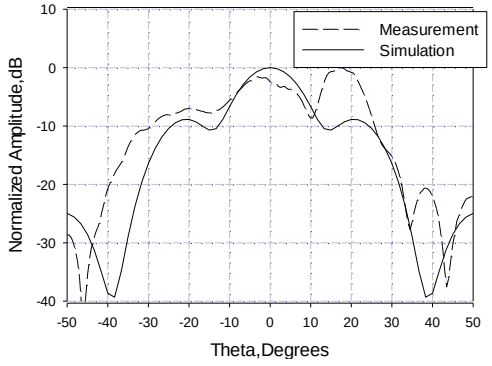

(a)

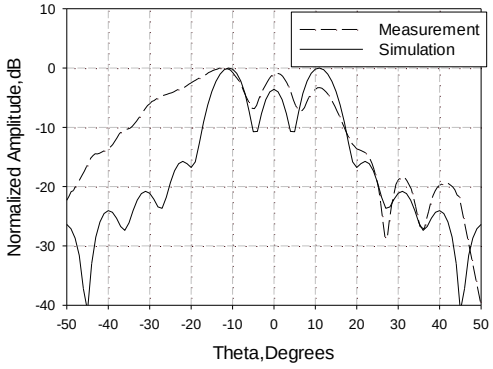

(b)

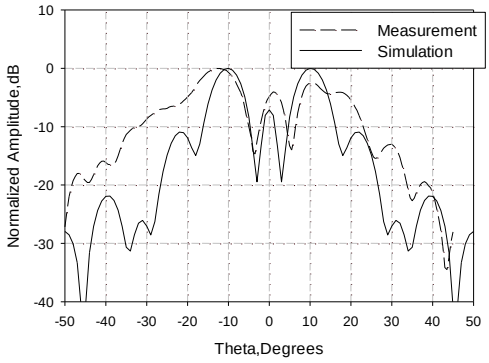

(c)

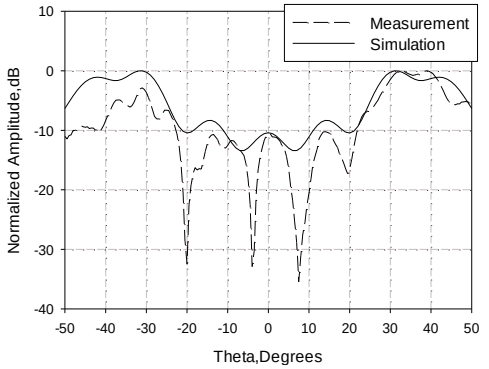

(d)

Fig. 12. Simulated and measured H-plane radiation patterns for: (a) 268GHz, (b) 270GHz, (c) 272GHz and (d) 302GHz.

6. Conclusion

A micromachined periodic surface based antenna has been proposed operating at low THz frequencies. An initial design for broadside operation at 284 GHz is presented. Moreover, at higher frequencies a split beam is obtained and a beam scanning application is proposed by changing the position of the feeding slot leading to a single beam operation. A prototype is fabricated and experimentally tested validating the simulations. The frequency shift compared to the original design is attributed to inaccuracies of the fabrication process which have a significant effect in this frequency band.

7. Acknowledgment

The authors would like to thank Dr. M. Henry from the Rutherford Appleton Laboratory, Didcot, U.K., for helping with the access and use of the radiation measurement system.

8. References

[1] Munk, B. A.: 'Frequency Selective Surfaces Theory and Design', (John Wiley, Hoboken, NJ, 2000)

[2] Padilla, W. J., Aronsson, M. T., Highstrete, C., Lee, M., Taylor, A. J., Averitt, R. D.: 'Novel Electrically Resonant Terahertz Metamaterials' Phys. Rev. B, Rapid 2007, 75, 041102

[3] Dickie, R., Cahill, R., Fusco, V., Gamble, H. S., Mitchell, N.: 'THz Frequency Selective Surface Filters for Earth Observation Remote Sensing Instruments', IEEE Trans. Terahertz Science and Technology, 2011, 1, (2), pp. 450-461

[4] Dickie, R., Cahill, R., Gamble, H. S., Fusco, V. F., Schuchinsky, A. and Grant, N.: 'Spatial demultiplexing in the sub-mm wave band using multilayer free-standing frequency selective surfaces', IEEE Trans. Antennas Propag., 2005, 53, (6), pp. 1903–1911

[5] Martin R. J. and Martin, D. H.: 'Quasi-optical antennas for radiometric remote sensing', Electron. Commun. Eng. J., 1996, 8, pp. 37–48

[6] Euler, M., Fusco, V. F., Cahill, R., and Dickie, R.: '325 GHz single layer sub-millimeter wave FSS based split slot ring linear to circular polarization convertor', IEEE Trans. Antennas Propag., 2010, 58, (7), pp. 2457–2459

[7] Argyropoulos, C., Le, K. Q., Mattiucci, N., D'Aguanno, G. and Alù, A.: 'Broadband Absorbers and Selective Emitters Based on Plasmonic Brewster Metasurfaces', Physical Review B, 2013, 87, (20), 205112-205117

[8] Debus, C., Bolívar, P. H.: 'Terahertz biosensors based on double split ring arrays', Proc. SPIE 6987, Metamaterials III, 2008, 69870U

[9] Llombart, N., Cooper, K. B., Dengler, R. J., Bryllert, T. and Siegel, P. H. 'Confocal ellipsoidal reflector system for a mechanically scanned active terahertz imager' IEEE Trans. Antennas and Propag., 2010, 99, (6), pp, 1834-1841

[10] Britton, J.W., Nibarger, J. P., Yoon, K.W., Beall, J. A., Becker, D., Cho, H.-M., Hilton, G. C., Hubmayr, J., Niemack, M. D. and Irwin, K. D.: 'Corrugated silicon platelet feed horn array for CMB polarimetry at 150 GHz', in SPIE Proc., 2010, 7741, p. 77410T

[11] Wu, Z., Liang, Min, Ng, Wei-Ren, Gehm, M., Xin, Hao: 'Terahertz Horn Antenna Based on Hollow-Core Electromagnetic Crystal (EMXT) Structure', IEEE Trans. Antennas and Propag., 2012, 60, (12), pp. 5557-5563

[12] Alonso-DelPino, M., Llombart, N., Chattopadhyay, G., Lee, C., Jung- Kubiak, C., Jofre, L. and Mehdi, I.: 'Design guidelines for a terahertz silicon micro-lens antenna', IEEE Antennas Propag. Lett., 2013, 12, pp. 84–87

[13] Filippovic, D. F., Gearhart, S. S. and Rebeiz, G. M.: 'Double slot on extended hemispherical and elliptical silicon dielectric lenses', IEEE Trans. Microw. Theory Tech., 1993, 41, (10), pp. 1738–1749

[14] Zhu, N. and Ziolkowski, R. W.: 'Progress toward THz antenna designs with high directivity and high efficiency', Antennas and Propagation Society International Symposium (APSURSI), 2013 IEEE, pp. 2271-2272

[15] Feresidis A. P. and Vardaxoglou, J. C.: 'High gain planar antenna using optimised partially reflective surfaces', IEE Proc. Microw. Antennas Propag., 2001, 148, (6), pp. 345-350

[16] Mateo-Segura, C., Feresidis, A. P. and Goussetis, G., ‘Bandwidth enhancement of 2-D leaky-wave antennas using double-layer periodic surfaces’, IEEE Trans. Antennas Propag., 2014, 62, (2), pp.586-593

[17] Trentini, G.V.: :Partially reflecting sheet array’, IRE Trans. Antennas Propag., 1956, AP-4, pp. 666-671

[18] Gardelli, R., Albani, M. and Capolino, F.: ‘Array thinning by using antennas in a Fabry-Perot cavity for gain enhancement’, IEEE Trans. Antennas Propag., 2006, 54, (7), pp. 1979-1990

[19] Mateo-Segura, C., Goussetis, G. and Feresidis, A. P.: ‘Sub-wavelength Profile 2-D Leaky-Wave Antennas with Two Periodic Layers’, IEEE Trans. Antennas Propag., 2011, 59, (2), pp. 416-424

[20] Muhammad, S. A., Sauleau, R. and Legay H.: ‘Small-Size Shielded Metallic Stacked Fabry–Perot Cavity Antennas With Large Bandwidth for Space Applications’, IEEE Trans. Antennas Propag., 2012, 60, (2) pp. 792-802

[21] Hosseini, S. A., Capolino, F., De Flaviis, F.: ‘A 44 GHz Single-Feed Fabry-Perot Cavity Antenna Designed and Fabricated on Quartz’, Int. IEEE Antennas and Propag. Symp. (AP-S), Spokane, WA, 4-8 July 2011

[22] Shang, X., Ke, M., Wang, Y. and Lancaster, M. J.: ‘Micromachined W-band waveguide and filter with two embedded H-plane bends’, IET, Microw., Antennas Propag., 2011, 5, (3), pp. 334-339

[23] Wang, Y., Ke, M., Lancaster, M.J., Chen, J.: ‘Micromachined 300-GHz SU-8-Based Slotted Waveguide Antenna’, IEEE Antennas Propag. Lett., 2011, 10, pp.573-576

[24] Shang, X., Ke, M., Wang, Y., Lancaster, M.J.: ‘WR-3 Band Waveguides and Filters Fabricated Using SU8 Photoresist Micromachining Technology’, IEEE Trans. Terahertz Science and Technology, 2012, 2, (6), pp.629-637